Volume 1 | Number 1 | Jan 2013 | Pages 1–100

ChemComm

Chemical Communications
www.rsc.org/chemcomm

ROYAL SOCIETY OF CHEMISTRY

ROYAL SOCIETY OF CHEMISTRY

www.rsc.org/chemcomm

Journal Name

ARTICLE

Coupled Chemical Oscillators and Emergent System Properties

Irving R. Epstein,[a]

We review recent work on a variety of systems, from the nanometre to the centimetre scale, including microemulsions, microfluidic droplet arrays, gels and flow reactors, in which chemical oscillators interact to generate novel spatiotemporal patterns and/or mechanical motion.

Introduction

The patterns produced by interacting oscillators have been of interest to scientists for at least half a millennium, since Huygens' classic experiments on the synchronization of pendulum clocks hung on a wall in proximity to one another[1]. Physicists have taken the lead in studying the behaviour of such systems, but chemists and biologists have become increasingly intrigued by the variety of phenomena that coupling two or more periodic entities may generate. In this Feature Article, I review work on a number of systems comprised of coupled chemical oscillators in which the characteristic size of the components may vary from a few nanometres to several centimetres.

In a sense, any reaction-diffusion system that contains an oscillatory chemical reaction may be viewed as a collection of coupled chemical oscillators, *i.e.*, pieces of the medium partitioned at any scale one likes, with the coupling provided by molecular diffusion. Such systems are undoubtedly interesting and can produce a remarkable variety of patterns[2], but here I shall focus on systems in which the oscillations occur not in a homogeneous medium but rather in what I shall refer to as "structured media": arrays of droplets, gels, and reactors.

All of the studies discussed in this article employ the Belousov-Zhabotinsky (BZ) reaction[3], the prototypical chemical oscillator. The term BZ reaction actually refers to a family of related reactions in which an organic substrate, most commonly malonic acid, is oxidised by bromate in a solution of strong acid (usually sulphuric or nitric) in the presence of a metal ion or metal complex that serves as a catalyst and usually as an indicator as well. The concentrations of the oxidised and reduced forms of the catalyst, along with those of several other species, *e.g.,* bromide, vary nearly periodically with a period typically of a few minutes. Although many other oscillating reactions are known, the vast majority of them oscillate only briefly, if at all, in the absence of a continuous inflow of fresh reactants. The Second Law of Thermodynamics requires that any closed system must proceed toward a stationary equilibrium state, thus precluding truly sustained oscillations. What makes the BZ reaction so attractive for studies of chemical pattern formation is that under appropriate conditions it will oscillate without replenishment for hundreds of cycles before the periodic behaviour ceases. In this respect it is unique among the known chemical oscillators, and only a handful of competitors[4-6] even come close.

The mechanism of the oscillatory BZ reaction was elucidated by Field, Körös and Noyes (FKN)[7]. They characterized the reaction in terms of three processes. In the first, Process A, the inhibitory species, Br^-, is consumed by BrO_3^-, generating a low steady state concentration of $HBrO_2$. The stoichiometric steps along with their rate laws are as follows:

$$BrO_3^- + Br^- + 2H^+ \rightarrow HBrO_2 + HOBr$$
$$v = k_1[BrO_3^-][Br^-][H^+]^2 \quad (A.1)$$
$$HBrO_2 + Br^- + H^+ \rightarrow 2HOBr$$
$$v = k_2[HBrO_2][Br^-][H^+] \quad (A.2)$$
$$HOBr + Br^- + H^+ \rightarrow Br_2 + H2O$$
$$v = k_3[HOBr][Br^-][H^+] \quad (A.3)$$
$$Br_2 + CH_2(COOH)_2 \rightarrow BrCH(COOH)_2 + Br^- + H+$$
$$v = k_4[Br_2][CH_2(COOH)_2] \quad (A.4)$$
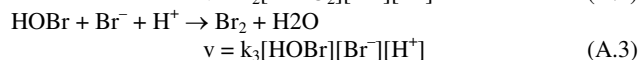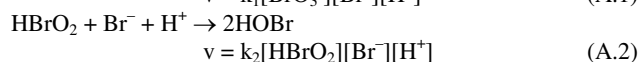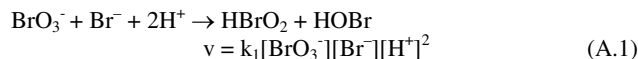
where the overall reaction is
$$BrO_3^- + 2Br^- + 3H^+ + 3CH_2(COOH)_2 \rightarrow 3BrCH(COOH)_2 + 3H_2O \quad (A)$$

Process A ceases when $[Br^-]$ falls below a critical value, allowing the autocatalytic production of bromous acid, $HBrO_2$, to take over in Process B. The catalyst system is generally represented as $M^{n+}/M^{(n+1)+}$. This couple can be, for instance, ferroin(II)/ferroin(III). Other catalysts include the Ce^{3+}/Ce^{4+} and Mn^{2+}/Mn^{3+} couples, as well as the photosensitive ruthenium *tris*-bipyridine complex discussed below. The stoichiometric steps of Process B with their empirical rate laws are:

$$HBrO_2 + BrO_3^- + H^+ \rightarrow 2BrO_2\bullet + H_2O$$
$$v = k_5[HBrO_2][BrO_3^-][H+] \quad (B.1)$$
$$BrO_2\bullet + M^{n+} + H^+ \rightarrow HBrO_2 + M^{(n+1)+}$$
$$v = fast \quad (B.2)$$
$$2HBrO_2 \rightarrow BrO_3^- + HOBr + H^+$$
$$v = k_6[HBrO_2]^2 \quad (B.3)$$
$$HOBr + CH_2(COOH)_2 \rightarrow BrCH(COOH)_2 + H_2O$$
$$v = k_7[HOBr][CH_2(COOH)_2] \quad (B.4)$$
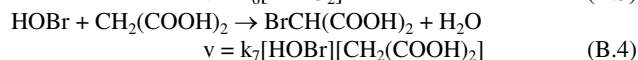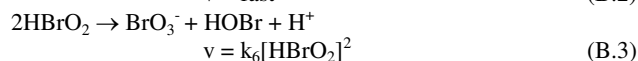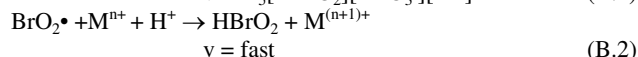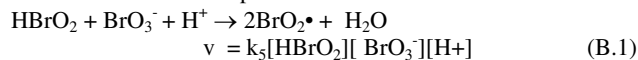
The overall reaction for Process B is
$$BrO_3^- + 5H^+ + CH_2(COOH)_2 + 4M^{n+} \rightarrow$$
$$BrCH(COOH)_2 + 4M^{(n+1)+} + 3H_2O \quad (B)$$
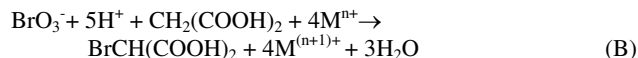
In process B there is net production of $HBrO_2$ and oxidization of the redox catalyst. It is also important to note that Process B is autocatalytic in $HBrO_2$, the concentration of which increases approximately six orders of magnitude above its steady state value reached in process A. When the oxidation of the reduced catalyst is essentially complete, the autocatalytic cycle ends, and process C takes control. Process C constitutes the "clock resetting," during which the catalyst is reduced and Br^- is regenerated:

$$4M^{(n+1)+} + BrCH(COOH)_2 + 2H_2O \rightarrow$$
$$4M^{n+} + 2CO_2 + HCOOH + 5H^+ + Br^- \qquad (C)$$
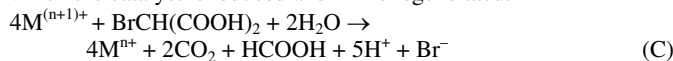
Once Process C has regenerated sufficient bromide, Process A is ready to begin again.

The net reaction consisting of the three processes is:

$$3\ BrO_3^- + 5\ CH_2(COOH)_2 + 3H^+ \rightarrow$$
$$3BrCH(COOH)_2 + 2HCOOH + 4CO_2 + 5H_2O \qquad (FKN)$$
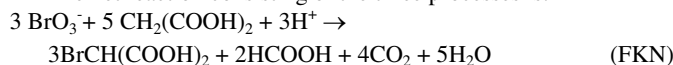
Results and discussion

I shall consider four types of structured media: so-called microemulsions, which actually consist of nanometre diameter water droplets immersed in a continuous oil phase; arrays of micrometre-sized water droplets in oil; gels that host the BZ reaction; and macroscopic flow reactors. Other kinds of media, such as membranes[8], ion exchange beads[9], phospholipids[10] or glasses[11], can also support fascinating behaviour in the BZ reaction, but these will not be discussed here.

BZ-AOT microemulsions

In an unstirred aqueous solution, the BZ reaction gives rise to traveling waves of concentration, which, if ferroin (Fe(1,10-phenanthroline)$_3$) is used as the catalyst, appear as propagating blue spirals or concentric waves ("target patterns") on a red background. If one adds an amphiphilic surfactant to an oil-water mixture, one can form a thermodynamically stable, isotropic mixture consisting of droplets of one phase surrounded by a monolayer of surfactant dispersed in a continuous phase of the other component. One of the most thoroughly studied such systems[12] consists of a simple hydrocarbon, *e.g.*, octane, water and the anionic surfactant sodium bis(2-ethylhexyl) sulfosuccinate, known as Aerosol OT, or simply AOT.

In an AOT-water-octane system with a relatively low [water]:[oil] ratio, one can form a reverse microemulsion, in which AOT-stabilised nanodroplets of water swim in a sea of oil. The BZ reactants and catalyst are polar, and if one places them in this mixture, they partition into the aqueous phase. Each aqueous droplet thus becomes a nanoscale BZ reactor. The droplets in such a system are quite monodisperse. Their mean radius in nm is given by[13] $R_w \approx 0.17\omega$, where $\omega =$ [H_2O]/[AOT]. We typically work in the range $10 < \omega < 25$, so our droplets are a few nanometres in diameter. One can also vary the average distance between droplets by changing the

[water]:[oil] ratio. When this ratio is increased enough, the droplets begin to coalesce into water channels; we have percolation, which is accompanied by a rise in the conductivity of the microemulsion of several orders of magnitude. Thus, by varying the relative amounts of oil, water and AOT, we have considerable control over the physical structure of the microemulsion. We can also manipulate the chemical characteristics of the system by choosing the concentrations of the BZ components: bromate, sulphuric acid, malonic acid (MA) and catalyst.

Because the droplets are so small, with volumes less than a zeptolitre (1 zL = 10^{-21} L), and the catalyst is typically present in millimolar concentrations, there are actually fewer catalyst molecules than water droplets. At any given moment, then, many of the droplets cannot support oscillation, because they lack catalyst. Also, because of the small numbers of molecules of all species present in a single droplet (just a few hundred even at 1 M concentration), one may expect large concentration fluctuations in each drop. Remarkably, the BZ-AOT system generates extremely regular patterns in time and space, with temporal periods similar to those observed in the aqueous BZ reaction and spatial wavelengths of the order of hundreds of micrometres, *i.e.*, tens of thousands of droplet diameters. Equally surprising, the variety of BZ-AOT patterns is far richer than that of the simple aqueous system, including a number of patterns that have yet to be observed in any other media.

Much of this behaviour, which is summarised in Figure 1, can be attributed to two features of the BZ-AOT system. First, because the droplets are so small, they undergo Brownian motion, moving through the oil, colliding with one another, and mixing their contents during those collisions through a coalescence-redispersion mechanism. Because the average time between collisions, about 1 ms, is much shorter than the period of oscillation, the medium can be treated as a continuous one. A second factor is that, although the BZ reactants and catalyst are essentially confined to the water droplets, the reaction generates less polar intermediates, Br_2 and BrO_2 in particular. The former acts as an inhibitor of the oscillatory behaviour, the latter as an activator. The apolar species can escape into the oil, move through it by diffusion, and occasionally enter another droplet, thus providing an alternative means to the collision-coalescence-redispersion process for communication between droplets. This movement of apolar single molecules occurs at rates one to two orders of magnitude faster than that of entire droplets, which contain tens of thousands of molecules, most of them water. Theory, dating back at least to Turing's seminal paper[14] on pattern formation, suggests that having multiple rates of diffusion enables a system to support a richer variety of patterns than a system in which all species diffuse at nearly the same rate.
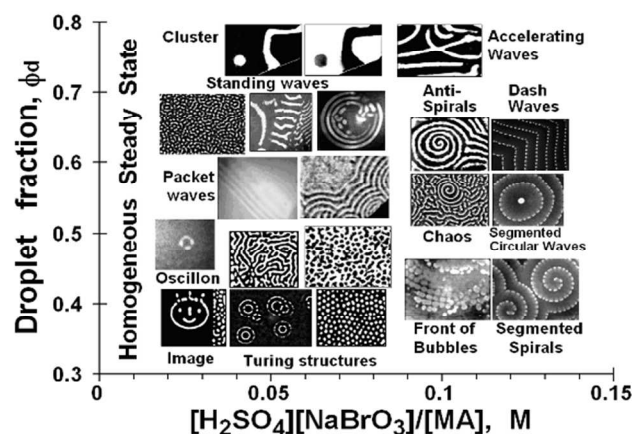
Fig. 1 "Phase diagram" showing patterns observed in the BZ-AOT system as parameters are varied. Vertical axis is volume fraction occupied by water droplets. Percolation occurs above about $\phi_d = 0.6$. Horizontal axis gives a measure of the oxidising power of the BZ reactant mixture.

Turing's analysis[14] requires that in order for an activator-inhibitor system to generate the stable, temporally stationary, spatially periodic patterns that he suggested as a mechanism for certain types of morphogenesis (and that now bear his name), the inhibitor must diffuse significantly faster than the activator. In simple aqueous solutions of monomeric species, nearly all ions and molecules have very similar diffusion coefficients. This seemingly trivial observation accounts for the fact that experimental efforts to produce Turing patterns were unsuccessful for nearly forty years after his work, until the serendipitous discovery[15] that reversible complexation of activator molecules by the starch indicator in the oscillatory chlorite-iodide-malonic acid reaction can produce the necessary difference of diffusion rates. The BZ-AOT system provides another case in which the diffusion of activator is slowed relative to that of inhibitor, here because under appropriate conditions relatively rapid diffusion through the oil phase is dominated by the inhibitory species, Br_2, while the predominant activator species are confined to the slower moving water droplets. The typical spots and stripes of Turing patterns are seen in a BZ-AOT system[16] just above the central portion of the horizontal axis in Figure 1.

Turing patterns were first predicted theoretically and were subsequently observed experimentally in other chemical systems. Several kinds of patterns, however, were first found or have thus far been seen only in the BZ-AOT system. We describe some of these here.

In the aqueous BZ system, as well as in many other chemical and biological systems, spiral waves are one of the most commonly occurring patterns. These waves originate from a central core, from which they propagate outwards at a constant velocity. These outwardly rotating spirals can also be found in the BZ-AOT system, but if one varies the composition, one finds a region of the parameter space in which, instead of

propagating out from their cores, spirals travel in from the periphery toward their centres[17]! We have dubbed these waves antispirals. Although the phenomenon had not previously been reported, theorists soon confirmed that the phenomenon occurs in a wide range of models[18-21] and is associated, as our model simulations suggested[22], with opposite signs for the group and phase velocities of the waves. More recently, antispirals have been reported in experiments on glycolytic oscillations in yeast[23].

A related phenomenon, which bears a superficial resemblance to wave packets in quantum mechanics, is the occurrence in the BZ-AOT system of packets of concentration waves that travel coherently through the medium. These packet waves[22], examples of which are shown in Figure 2, may propagate either toward or away from their centre of curvature, depending on whether their group velocity is positive or negative. They range from nearly plane waves to target-like patterns.
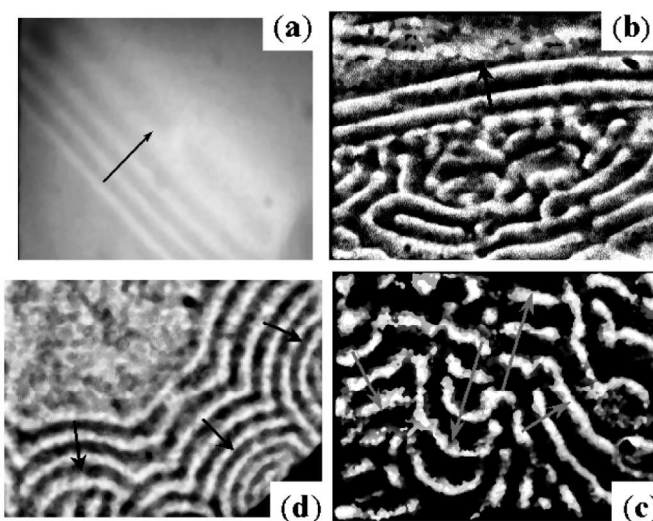
Fig. 2 Packet waves in the BZ-AOT system[22]. a) plane wave-like packets, frame size = 2.5 mm x 2.2 mm; b),c) a single experiment in which plane waves initially form the boundary of a chaotic region (b), which subsequently evolves (c) into adjacent wave packets moving in opposite directions, size = 1.88 mm x 1.4 mm; (d) target-like packet waves, size = 3.76 mm x 2.81 mm. Arrows mark direction of wave propagation.

Under certain conditions, packet, target or spiral waves may undergo a transverse instability, which causes the waves to break into smaller segments. These small segments, or dashes, propagate coherently in a direction perpendicular to that of the breaks. In the case of nearly plane waves, they form "dash waves[24]," lines of propagating dashes that increase in length as they move, until they reach a critical size, at which point they split into two, continuing to propagate, grow and split. The phenomenon is most striking in the case of spiral waves[25], as illustrated in Figure 3. Figure 3a shows the onset of segmented spiral formation, as a set of dash waves approaches from the right, causing the spiral to begin to break into dashes near its

core. The spiral propagates outward by a process in which the dashes lengthen, reach the critical size, and split, eventually taking over the entire spiral structure. Figure 3b shows a pair of fully developed segmented spirals.
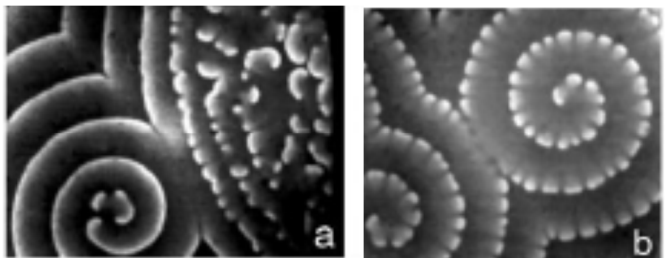
Fig. 3 Segmented spirals in a BZ-AOT microemulsion[25]. a) Birth of a segmented spiral (left) from an ordinary spiral on which dash waves impinge. b) a pair of segmented spirals. Frame size 3.8 mm x 5.0 mm.

The patterns discussed above are all essentially two-dimensional. The experimental medium consists of a thin layer (ca. 0.1 mm) of microemulsion sandwiched between a pair of glass plates. The thickness of the layer is less than the wavelength of the patterns, so pattern formation can occur only parallel to the glass surfaces. Theoretical considerations suggest that additional patterns should arise in a three-dimensional medium[26]. The challenge is how to visualize them, since simply looking at the medium by eye or with an ordinary microscope will yield a two-dimensional projection that is likely to obscure the pattern being sought. One solution to this problem is to apply tomographic techniques, similar to those used by radiologists to obtain three-dimensional scans of the human body. In this approach, one takes a series of two-dimensional snapshots from different angles and then combines them using an appropriate algorithm to construct a three-dimensional image. Figure 4 shows the first such images of three-dimensional patterns in the BZ-AOT system[27].
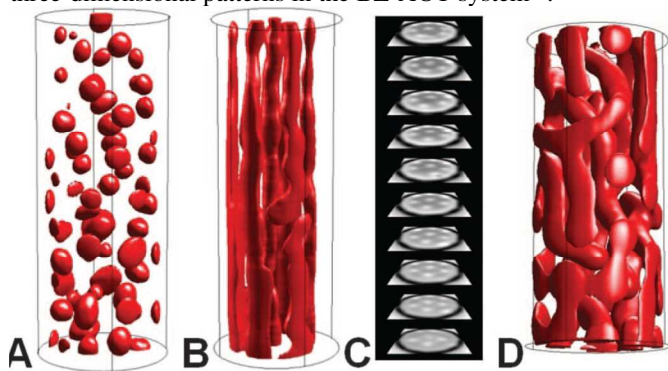
Figure 4 Tomographically reconstructed concentration fields of three-dimensional Turing patterns[27]. (A) spots; (B) hexagonally close-packed tubes; (C) horizontal cross sections through the data in (B); (D) intertwined tubes. Capillary inner diameter = 0.6 mm.

The experiments are done by placing the microemulsion in a cylindrical quartz capillary with an inner diameter (0.3–0.6 mm) that exceeds the wavelength of the anticipated structures. The capillary is rotated at 0.25 revolutions per second, and absorption images are taken at a rate of 20 frames per second. The 2D images from a full revolution are then processed to give a single 3D image. Although the technique is still in its infancy, and Turing patterns are the easiest to image, since they are stationary in time, the initial results are quite promising. We have recently obtained results on standing wave patterns[28] as well.

We conclude this section by noting that, because the BZ-AOT medium behaves in most important respects as if it were a continuum, we are able to simulate, at least qualitatively, essentially all of the patterns we have observed to date with relatively simple models[16, 29] based on well-established, mechanistically sound models[30, 31] for the aqueous BZ reaction. Essentially, our BZ-AOT models consist of two- to four-variable reaction-diffusion (partial differential equation) models of the aqueous BZ reaction augmented by, depending on the circumstances, one or two variables that describe the nonpolar species, Br_2 and/or BrO_2, in the oil phase. To take into account the fact that the species in the oil move as single molecules, while those in the droplets travel together with the entire droplet, the diffusion coefficients of the nonpolar species are taken to be an order of magnitude or more greater than those of the species confined to the droplets. All of the chemistry occurs within the droplets. The only "reactions" undergone by the nonaqueous species are diffusion through the oil, entrance into the oil at a rate proportional to the concentration of its aqueous precursor (Br^- for Br_2, $HBrO_2$ for BrO_2), and departure from the oil at a rate proportional to its own concentration. Although these transfer rates are not known, they can be estimated, and their ratios are given by the partition coefficients for the relevant species.

Droplet arrays

The BZ-AOT system is a powerful one, but it suffers from important limitations, particularly if we wish to be able to manipulate our patterns. Because the droplets are so small, the detailed structure of the microemulsion actually plays a relatively minor role. As noted above, for most purposes the fact that the interdroplet exchange occurs on a much faster time scale than the oscillatory chemical reaction means that the system behaves (and can be modelled as) a continuous one. We are unable to observe individual droplets or to select a particular droplet or set of droplets to perturb. In fact, because of the constant motion and collisions, even the notion of the identity of a single droplet is problematic. The coupling between droplets, which depends on the diffusion either of whole droplets or of single oil-soluble molecules, lies beyond the experimenter's ability to control. An alternative approach is to construct a system composed of distinct droplets that remain in a single location, can be individually seen and addressed, and can be arranged in a selected topology and with distances, and

hence coupling strengths, subject to the experimenter's choice, at least within certain limits. In this section, we describe how this goal may be accomplished with the use of microfluidics.

We have carried out experiments in both one- and two-dimensional configurations. The 1D arrangement, shown in Figure 5, employs two capillaries, one filled with aqueous BZ solution, the other with octane and a small amount of surfactant[32]. The two liquids are driven into a microfluidic junction by syringe pumps (Figure 5a). When they meet, the BZ solution forms a stream of monodisperse, equally spaced drops that are carried along by the continuous oil stream. The size of and separation between the droplets depend upon the junction size and the flow rates of the two streams. The experiments employ ferroin, which is red in its reduced state and blue in its oxidised state, as the primary catalyst, with a small amount of ruthenium tris(2,2'-bipyridine) (Ru(bipy)$_3$) added as a co-catalyst and photosensitizer. When the Ru(bipy)$_3$-containing BZ solution is illuminated with a strong 450 nm light source, all the catalyst is reduced. We utilize this feature both to initialize the experiments by illuminating the entire capillary to put all drops in the same state and, as described below, to selectively perturb individual drops in a pattern.
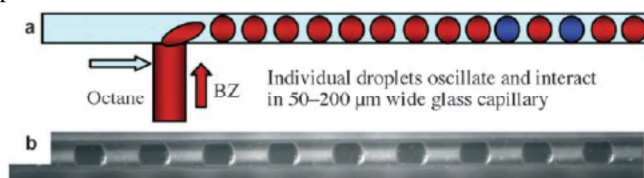
Fig. 5 1D microfluidic configuration[32]. a) Schematic representation of the microfluidic device. Red droplets correspond to the reduced form of the catalyst (ferroin), blue droplets to the oxidised form (ferriin). b) Snapshot of a capillary with droplets. BZ droplets with convex surfaces are dark due to ferroin. Horizontal length of the frame and inner diameter (ID) of the capillary are 4.8 mm and 150 μm, respectively. BZ droplets were recorded by a CCD camera through a microscope with illumination by light passed through a 510 nm interference filter.

Under the conditions of our experiments, the dominant species in the oil phase is the inhibitor, bromine. The coupling between drops is therefore negative. As a result, the most commonly observed patterns, seen as space-time plots in Figure 6, are either antiphase oscillations, in which the spike of oxidation in each drop's cycle occurs 180° out of phase relative to the spikes in its adjacent drops, or 1D Turing patterns, in which drops alternate between oxidised and reduced stationary states. The plots are constructed by taking a series of snapshots along the central axis of the capillaries shown at the top of Figure 6 and stacking them along the time axis. The bright vertical lines are the oil drops that separate the BZ drops in which the reaction occurs. More complex 1D patterns consisting of mixtures of stationary and oscillatory drops or containing short sequences of in-phase neighbours can also occur in some parameter ranges[33].
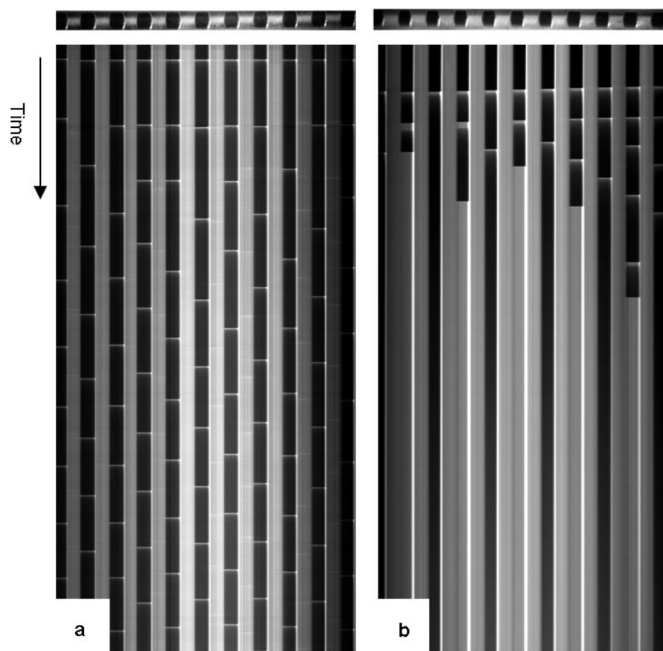
Fig. 6 Space–time plots[32] showing a) anti-phase oscillations with spikes of oxidation of ferroin seen as light horizontal lines across BZ droplets and b) stationary Turing structures with alternating oxidised and reduced states evolving from an initial oscillatory state. Horizontal lengths of the frame and the capillary inner diameter are 4.8 mm and 150 μm, respectively; the total times for (a) and (b) are 5200 s and 10800 s, respectively. Patterns extend to the left and right of the segments shown.

The phenomenology in two dimensions is considerably richer than in 1D[33]. When placed between a pair of flat plates and packed at high density, the drops spontaneously self-assemble into a hexagonal array with a few defects. The hexagonal geometry, with each drop having six nearest neighbours, makes it impossible for the system to take on the alternating antiphase or Turing behaviour preferred in 1D. Instead, the two most prevalent patterns arising out of the geometrical constraint are a) a mixed stationary-oscillatory state, denoted π-S, in which one third of the drops are stationary, and each stationary drop is surrounded by a hexagon of oscillating drops, each antiphase with its oscillating neighbours; and b) an oscillatory state, labelled 2π/3, in which each drop is 120° out of phase with the drops adjacent to it. The π-S and 2π/3 states are illustrated in Figures 7 and 8, respectively. Stronger coupling, i.e. smaller drops or lower [MA], favors the π-S state over the 2π/3 state. The exact nature of the coupling is a nontrivial problem, and we have explored it in some detail in model calculations[34, 35].

In a recent set of experiments[36], we have used two-dimensional arrays of BZ drops to re-examine some of Turing's predictions[14] about morphogenesis. Turing analysed the behaviour of a ring of identical "cells," each undergoing a set of
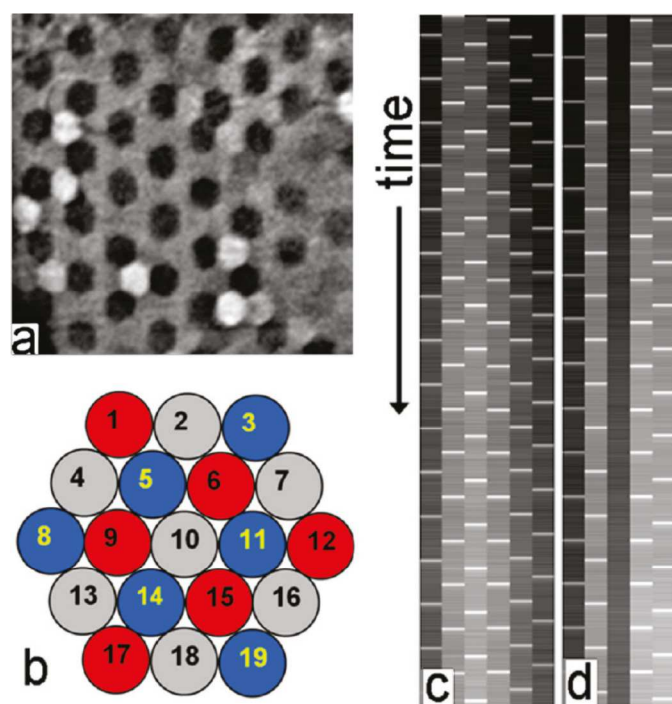
Fig. 7 The π-S state[33]. (a) Hexagonally packed drops forming a larger hexagon with each stationary drop (black) surrounded by six oscillatory drops. Imaged area is 0.7 x 0.7 mm. (b) Schematic representation of the pattern (stationary drops in gray; red and blue denote opposite phases of oscillatory drops). (c,d) Space-time plots (duration 2800 s) of drops 6, 11, 15, 14, 9, and 5 (c) and drops 1, 5, 10, 15, and 19 (d).

"chemical reactions." By using light to suppress reaction in all but a ring of cells in our hexagonal array, we can isolate a group of BZ drops and monitor their behaviour. The existence of defects enables us to select rings containing as few as four or as many as nine drops in additional to the more common six-membered rings. Turing actually identified six instabilities that lead to pattern formation in such systems, and we have found them all experimentally. Moreover, we have been able to demonstrate mathematically that the π-S state, which cannot be accounted for by Turing's linear stability analysis, requires the existence of inhomogeneity; it cannot arise if all the droplets are identical. This requirement is, of course, easily satisfied in any experiment, where small differences in drop size or composition are inevitable.

The most exciting result obtained in our study is a verification of Turing's prediction that the chemical differentiation arising from the instabilities produced by the interaction of the reaction kinetics and intracellular diffusion can lead to physical morphogenesis. This result is demonstrated in Figure 9, where the drops, which are initially nearly homogeneous in both size and chemical composition, first undergo a chemical change to produce a Turing pattern consisting of a mixture of drops in oxidised and reduced steady states. After a bit more than an hour, as the result of osmosis (the reduced and oxidised states have different osmolalities),

the reduced drops grow and the oxidised drops shrink, resulting in two morphologically different groups of cells.
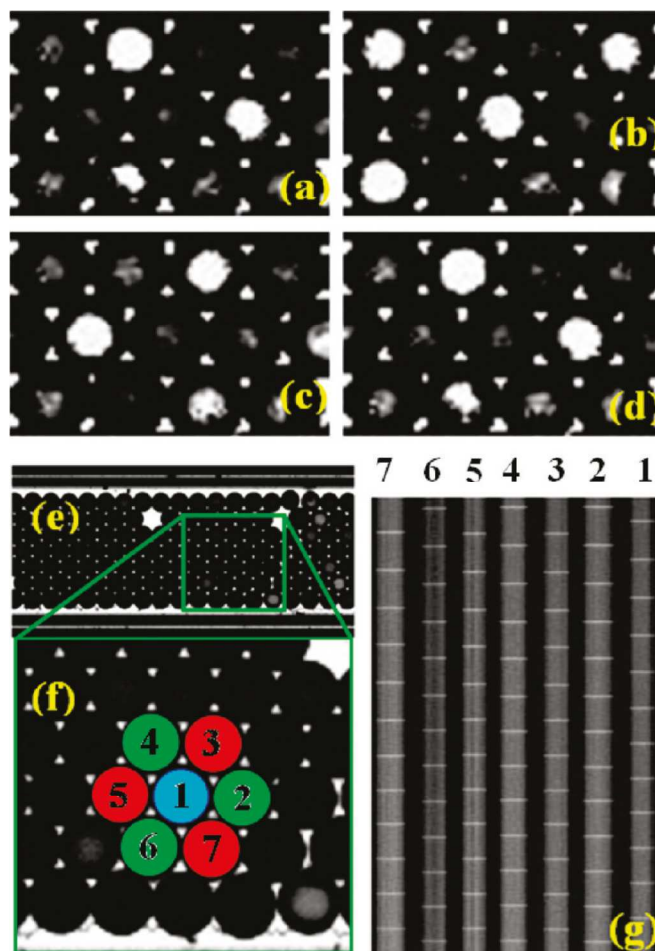
Fig. 8 The 2π/3 state[33]. Snapshots a-d are taken at t=0, T/3, 2T/3, and T, where T = 231 s. Snapshot e and its enlargement (f) show a 2D configuration of BZ drops. (g) Space-time plot for drops 1-7 shown in snapshot f; dimensions are 896 μm horizontal and 2877 s vertical. Period of oscillations for each drop in the space-time plot is the same as T in snapshots a-d.

As in the case of the BZ-AOT system, it is relatively easy to simulate the behaviour of our 1D and 2D arrays of coupled drops using models developed for the homogeneous aqueous BZ system. Although, as noted above, the details of the coupling are not straightforward, we have been able to achieve good agreement with experiment using plausible models that take into account the droplet size and spacing, the partition coefficients of the relevant species, and the effect of malonic acid on the concentrations of key bromine species involved in interdrop transport[34, 35].
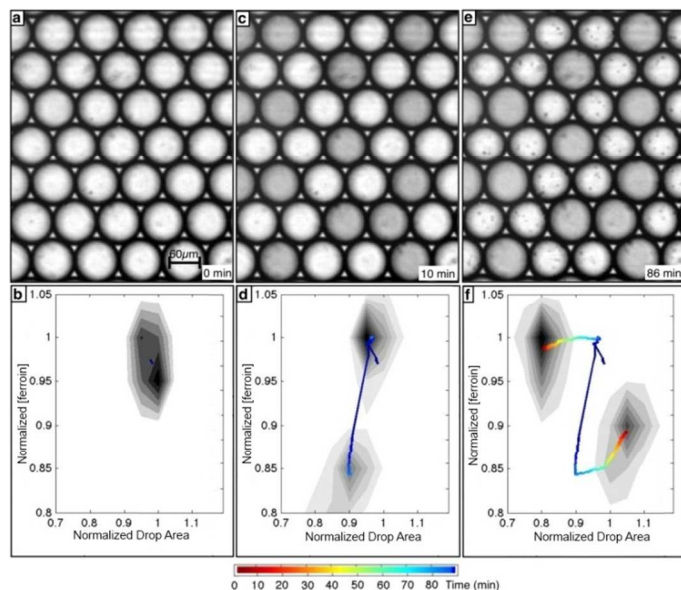
Fig. 9 Images (upper row) and histograms (lower row) of drops demonstrating morphogenesis[36]. Histograms show fraction of original concentration of reduced BZ catalyst *vs.* fraction of original drop area. Grey scale in histograms is proportional to the number of drops with a given area and intensity. Color coded lines track the centre of each peak as a function of time. (**a,b**) Initially, drops are nearly homogeneous in both intensity and size. (**c,d**) At intermediate times, drops undergo a Turing bifurcation, becoming heterogeneous in oxidation state, but remaining homogeneous in size, as seen by the differentiation into lighter and darker drops. (**e,f**) Later, drops become heterogeneous in both oxidation state and size. The oxidised (brighter) drops shrink and the reduced drops swell.

BZ Gels

Much of the chemical energy produced in our bodies *via* the hydrolysis of ATP is used to generate mechanical force in muscle. One might ask whether the chemical energy in a chemical oscillator might be transduced into mechanical motion as well. Yoshida[37] made a major breakthrough in this direction by covalently attaching the BZ catalyst $(Ru(bipy)_3)$ to the polymer poly(N-isopropylacrylamide) (poly(NIPAAm)). When cross-linked to form a gel and placed in a solution containing bromate, MA and nitric acid, the polymer periodically shrinks and swells with the oscillations in the oxidation state of the BZ catalyst. The oxidised form of the catalyst attracts water into the gel, which expands; during the reduced portion of the oscillatory cycle, water leaves and the gel shrinks[38]. Yoshida and his coworkers have exploited these BZ gels to build a number of clever systems, including one in which the reactants as well as the catalyst of the BZ reaction are attached to the gel[39] and another in which the peristaltic motion generated by the gel oscillations is used to transport small objects[40]. Balazs and collaborators have developed a powerful computational package that combines a simple model for the BZ chemistry

with a gel lattice spring model[41] that describes the elastodynamics of BZ gels. Their simulations give excellent qualitative agreement with a wide range of experiments on these systems[42].

Much of our own work on BZ gels has been directed at exploring how the structure of the BZ catalyst may be modified to change the properties of the gel, with the ultimate goal of optimizing the functionality of these intriguing materials. In one study[43], we synthesised two variants of the Yoshida catalyst, in which the length of the segment that links the ruthenium catalyst to the poly(NIPAAm) backbone was increased from 1.52 Å to as much as 11.2 Å. We found that this molecular manipulation enables one to tailor such features as the initiation time, frequency of oscillation and volume change of BZ hydrogels and to better understand the structure-function relationships in these materials.

In the Yoshida gel, polymer chains are crosslinked by the bifunctional molecule, *N,N'*-methlyenebis(acrylamide) (BIS), which does not undergo further chemical activity once the crosslink is formed. The $Ru(bipy)_3$ catalyst is attached as a pendant to the polymer chain. In many biopolymer networks, in contrast, the crosslinker is *active*. For example, in the cytoskeleton of muscle cells, actin filaments are crosslinked by active myosin motors[44]. In an effort to mimic this phenomenon in a BZ gel, we modified the catalyst by replacing the bipy ligands by N,*N'*-diallyl-(2,2'-bipyridine)-4'4'-dicarboxamide, which preserves the catalytic function while allowing the catalyst molecule to form up to six covalent bonds to the polymer chain, thereby eliminating the need for a separate crosslinker[45]. Because of the multidentate nature of the crosslinker, the resulting gel has a fully three-dimensional structure. Remarkably, in contrast to the Yoshida gel, it shrinks in the oxidised state and swells in the reduced state, and the volume change is significantly increased. We attribute these results to the active nature of the crosslinks, i.e., to the fact that their strength and geometry changes with the oxidation state of the catalyst. The process is shown schematically in Figure 10.

In other studies, we have examined how post-self-assembly crosslinking may be employed to integrate molecular nanofibers of hydrogelators with BZ copolymers to produce oscillatory gels with larger pore sizes or other desirable chemical or mechanical properties[46, 47].
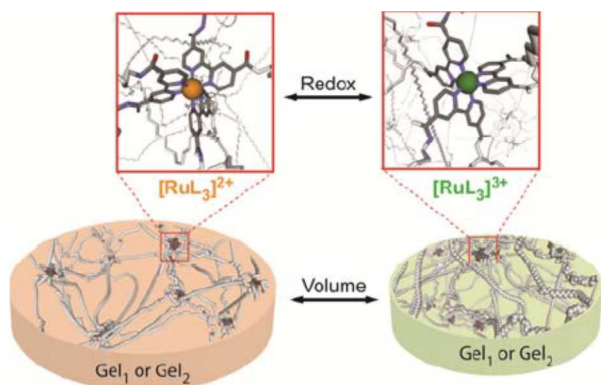
Fig. 10 Conceptual illustration of active BZ gel with volumetric oscillation induced by the redox oscillation of the active crosslinker[45]. Polymer sidechains are omitted for clarity.

The photosensitivity of BZ gels offers promise for future applications. The ruthenium catalyst absorbs light in a region around 450 nm, resulting in suppression of oscillations above a threshold level of illumination. Balazs incorporated this photoinhibition into her model and predicted that one should be able to construct a photophobic "worm," a piece of BZ gel that could be made to move in a preselected path by manipulating a pattern of illumination[48]. We carried out experiments[49] on pseudo-one-dimensional BZ gels in capillary tubes and found not only the photophobic behavior predicted by the simulations but, at different levels of illumination, *phototropic* behavior as well. The experiment consists of illuminating half the capillary at one intensity and the other half at a different intensity. The simulations, which assume that the frequency of oscillation decreases with light intensity, predict that the gel should move toward the darker (higher frequency) end of the tube. In the experiments, we found, surprisingly, that the frequency actually passes through a maximum as a function of light intensity, so that if both halves of the capillary are exposed to intensities below the maximum, the brighter half will have higher frequency and will thus be more attractive to the "gel worm." The experimental results are illustrated in Figure 11.
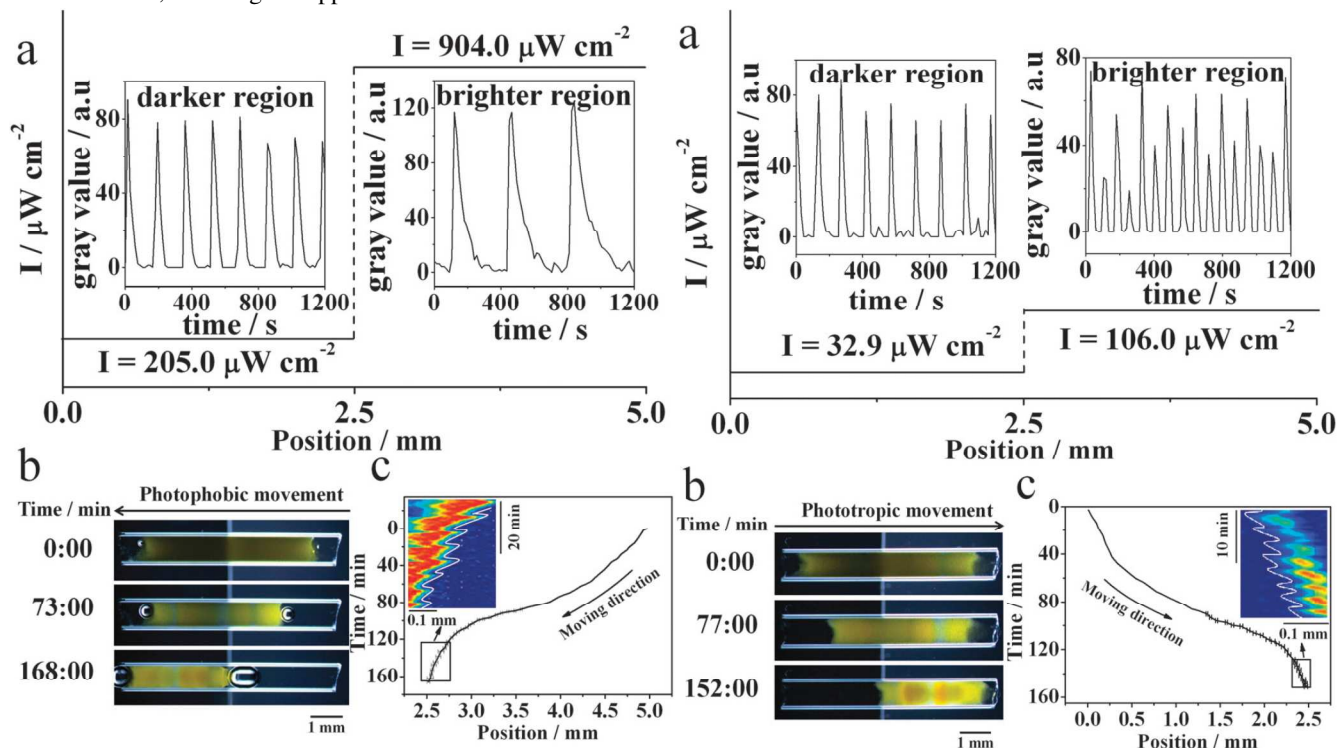
Fig. 11. Phototropic and photophobic movement of BZ photosensitive gels in a capillary under spatially nonuniform illumination[49]. Left frames show photophobic behavior at light intensities above the maximum in frequency. Right frames show phototropic motion below the maximum. In each set, (a) shows the distribution of light intensity and the local oscillation in grey value (proportional to concentration of oxidised catalyst); (b) shows snapshots of gel (yellow region) movement; (c) shows location of left edge of the gel *vs.* time. The motion exhibits small amplitude oscillations superimposed on the net phototactic movement. These are seen in the insets to the (c) panels.

Pulse-Coupled Reactors

At a very different length scale, chemists have been studying the behaviour of coupled chemical oscillators in macroscopic continuous flow stirred tank reactors (CSTR) for several decades[50-53]. The reactors are generally coupled by mass flow through tubes or membranes that connect them to each other. In a CSTR, one feeds a constant stream of reactants into the reactor, and there is an outflow tube through which reacted material leaves the system, keeping the volume constant. Instead of looking at zeptolitre or nanolitre volumes, one typically deals with reactors containing tens of millilitres. It is relatively straightforward to introduce one or more probes, usually potentiometric or spectrophotometric, into each reactor and to perturb it with light or by the addition of chemicals. The flows maintain the system in an open, far-from-equilibrium state, so that, in principle, the oscillations can continue indefinitely. The tradeoff is that it is experimentally quite challenging to couple more than a handful, often just two, CSTRs in this fashion.

In this section, we describe recent experiments on a novel variant of coupled CSTRs, in which the coupling occurs by brief injections into one reactor, in response to a prespecified concentration change in another reactor, of a species that tends to either induce or suppress oscillations. The system is designed to mimic some aspects of a set of synaptically coupled neurons.

Figure 12 shows a single CSTR in this system. The BZ reactants and catalyst are fed in from two reservoirs by a peristaltic pump. The reactor is equipped with a platinum redox electrode and a reference electrode, allowing us, with the aid of the pH meter and a data acquisition setup, to monitor the electrochemical potential of the system. Each reactor is connected *via* a solenoid valve with reservoirs containing either KBr, which inhibits oscillation, or $AgNO_3$, which excites oscillation. When, as the result of an oxidation spike, the potential in a CSTR rises above a threshold set by the experimenter, a signal is generated. This signal initiates the opening of solenoid valves in those CSTRs that are coupled to the spiking reactor. The sign of the coupling, which is controlled by the experimenter, is determined by whether bromide or silver ion is released. The magnitude of the coupling can be controlled as well by setting the concentrations in the reservoirs and/or the duration of the short period for which the valve remains open (the pulse length). The system incorporates several characteristics of synaptically coupled neurons: coupling may be excitatory or inhibitory, depending on the identity of the "neurotransmitter" emitted by the presynaptic cell; transmission of information is pulsatile, rather than continuous as in diffusively coupled oscillators; each pair of oscillators may be coupled unidirectionally or bidirectionally; the pulse to the postsynaptic cell need not be delivered instantaneously, but may reach its destination only after a delay (in our system, this delay can be set in the controlling software).
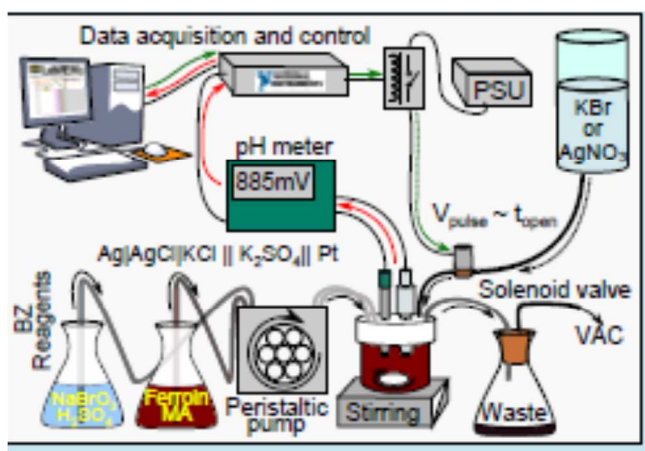
Fig. 12 Schematic diagram of experimental apparatus for pulse-coupled BZ oscillators[54].

We have carried out extensive experiments on a pair of pulse-coupled BZ oscillators with all combinations of excitatory and inhibitory coupling, with and without delays[54]. Even in this very simple configuration, the variety of patterns obtained is impressive. The observed behaviours include in-phase and antiphase oscillations; complex oscillations, in which one oscillator spikes m times followed by n spikes of the other oscillator; bursting, in which trains of fast oscillations alternate with quiescent periods; and suppression, whereby one CSTR oscillates while the other exhibits a constant potential. Some examples of these patterns, all of which we have been able to simulate qualitatively with simple models, are shown in Figure 13. We are currently studying the behaviour of sets of three and four pulse-coupled BZ oscillators. The number of possible combinations of connective topology and signs of coupling grows exponentially with the number of CSTRs. We are focusing our attention on configurations that may lend insight into some relatively simple neural networks, such as the crustacean stomatogastric ganglion[55].
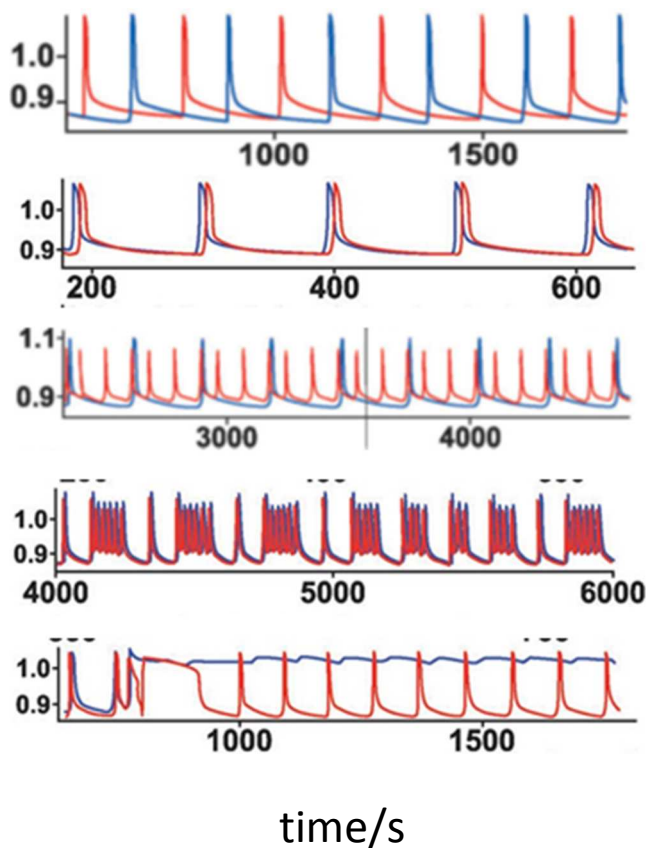
Fig. 13 Traces of experiments on two pulse-coupled BZ oscillators. Vertical axis is electrochemical potential (V); Blue and red traces represent the two reactors. From top: antiphase oscillations, mutual inhibitory coupling, no delay; nearly in phase oscillations, mutual excitatory coupling, no delay; complex (3:1) oscillation, mixed excitatory-inhibitory coupling, 25 s delay; bursting, mutual excitatory coupling, 5 s delay; suppression, mutual excitatory coupling, 35 s delay.

Conclusions

A plausible definition of systems chemistry is that it is the study of how chemical entities, each capable of nonlinear dynamical behaviour on its own, interact so as to produce more complex patterns of behaviour that allow for increased functionality. The oscillatory BZ reaction in a variety of structured media produces a striking variety of spatiotemporal behaviours, many of them reminiscent of phenomena in biology. The experiments described here are only a start toward exploiting the potential applications of combining chemical oscillation with self-organization, mechanics, and transport phenomena such as diffusion, osmosis and convection. Living organisms, which have had eons to figure out how to do this sort of systems chemistry, serve as an inspiration to all of us working on these problems.

Acknowledgements

Notes and references

[a] Department of Chemistry and Volen National Center for Complex Systems, MS 015, Brandeis University, Waltham, MA 02454. E-mail: epstein@brandeis.edu

1. A. Pikovsky, M. Rosenblum and J. Kurths, *Synchronization: A Universal Concept in Nonlinear Sciences*, Cambridge University Press, New York, 2011.
2. I. R. Epstein and J. A. Pojman, *Introduction to Nonlinear Chemical Dynamics: Oscillations, Waves, Patterns and Chaos*, Oxford University Press, New York, 1998.
3. A. M. Zhabotinsky, *Biofizika*, 1964, **9**, 306-311.
4. W. C. Bray, *J. Am. Chem. Soc.*, 1921, **43**, 1262-1267.
5. T. S. Briggs and W. C. Rauscher, *J. Chem. Ed.*, 1973, **50**, 496.
6. P. De Kepper, I. R. Epstein, K. Kustin and M. Orbán, *J. Phys. Chem. A*, 1982, **86**, 170-171.
7. R. J. Field, E. Körös and R. M. Noyes, *J. Am. Chem. Soc.*, 1972, **94**, 8649-8664.
8. D. Winston, M. Arora, J. Maselko, V. Gaspar and K. Showalter, *Nature*, 1991, **351**, 132-135.
9. J. Maselko and K. Showalter, *Physica D*, 1991, **49**, 21-32.
10. G. Biosa, S. Ristori, O. Spalla, M. Rustici and M. J. B. Hauser, *Journal of Physical Chemistry A*, 2011, **115**, 3227-3232.
11. I. R. Epstein, I. Lengyel, S. Kadar, M. Kagan and M. Yokoyama, *Physica A*, 1992, **188**, 26-33.
12. T. K. De and A. Maitra, *Adv. Colloid Interface Sci.*, 1995, **59**, 95 - 193.
13. M. S. Baptista and C. D. Tran, *Journal of Physical Chemistry B*, 1997, **101**, 4209-4217.
14. A. M. Turing, *Philos. Trans. R. Soc. London Ser. B*, 1952, **237**, 37-72.
15. V. Castets, E. Dulos, J. Boissonade and P. De Kepper, *Phys. Rev. Lett.*, 1990, **64**, 2953-2956.
16. V. K. Vanag and I. R. Epstein, *Phys. Rev. Lett.*, 2001, **87**, 228301.
17. V. K. Vanag and I. R. Epstein, *Science*, 2001, **294**, 835-837.
18. Y. F. Gong and D. J. Christini, *Phys. Rev. Lett.*, 2003, **90**, 088302.
19. Y. F. Liu, Y. N. Wu, H. J. Xu and J. F. Sun, *Comm. Theor. Phys.*, 2004, **42**, 637-640.
20. E. M. Nicola, L. Brusch and M. Bär, *Journal of Physical Chemistry B*, 2004, **108**, 14733-14740.
21. H. L. Wang and Q. Ou-Yang, *Chinese Physics Letters*, 2004, **21**, 1437-1440.
22. V. K. Vanag and I. R. Epstein, *Phys. Rev. Lett.*, 2002, **88**, 088303.
23. R. Straube, S. Vermeer, E. M. Nicola and T. Mair, *Biophysical Journal*, 2010, **99**, L4-L6.

24. V. K. Vanag and I. R. Epstein, *Phys. Rev. Lett.*, 2003, **90**, 098301.

25. V. K. Vanag and I. R. Epstein, *Proc. Natl. Acad. Sci. U. S. A.*, 2003, **100**, 14635-14638.

26. A. DeWit, P. Borckmans and G. Dewel, *Proc. Nat. Acad. Sci. U.S.A.*, 1997, **94**, 12765-12768.

27. T. Bánsági Jr., V. K. Vanag and I. R. Epstein, *Science*, 2011, **331**, 1309-1312.

28. T. Bansagi Jr., V. K. Vanag and I. R. Epstein, *Physical Review E*, 2012, **86**, 045202.

29. V. K. Vanag and I. R. Epstein, *J. Chem. Phys.*, 2009, **131**, 104512-104511-104517.

30. R. J. Field and R. Noyes, *J. Chem. Phys.*, 1974, **60**, 1877-1884.

31. J. J. Tyson and P. C. Fife, *J. Chem. Phys.*, 1980, **73**, 2224-2237.

32. M. Toiya, V. K. Vanag and I. R. Epstein, *Angewandte Chemie-International Edition*, 2008, **47**, 7753-7755.

33. M. Toiya, H. O. González-Ochoa, V. K. Vanag, S. Fraden and I. R. Epstein, *J. Phys. Chem. Lett.*, 2010, **1**, 1241-1246.

34. V. K. Vanag and I. R. Epstein, *Phys. Rev. E*, 2011, **84**, 066209-066201-066215.

35. V. K. Vanag and I. R. Epstein, *J. Chem. Phys.*, 2003, **119**, 7297-7307.

36. N. Tompkins, N. Li, C. Girabawe, M. Heymann, G. B. Ermentrout, I. R. Epstein and S. Fraden, *Proc. Nat. Acad. Sci. USA*, 2014, **111**, 4397-4402.

37. R. Yoshida, H. Ichijo, T. Hakuta and T. Yamaguchi, *Macromol. Rapd Commun.*, 1995, **16**, 305-310.

38. R. Yoshida, T. Takahashi, T. Yamaguchi and H. Ichijo, *J. Amer. Chem. Soc.,* 1996, **118**, 5134-5135.

39. Y. Hara, T. Sakai, S. Maeda, S. Hashimoto and R. Yoshida, *J. Phys. Chem. B*, 2005, **109**, 23316-23319.

40. Y. Murase, S. Maeda, S. Hashimoto and R. Yoshida, *Langmuir*, 2009, **25**, 483-489.

41. V. V. Yashin and A. C. Balazs, *J. Chem. Phys*, 2007, **126**, 124707.

42. O. Kuksenok, P. Dayal, A. Bhattacharya, V. V. Yashin, D. Deb, I. C. Chen, K. J. Van Vliet and A. C. Balazs, *Chem. Soc. Rev.*, 2013, **42**, 7257-7277.

43. Y. Zhang, N. Li, J. Delgado, N. Zhou, R. Yoshida, S. Fraden, I. R. Epstein and B. Xu, *Soft Matter*, 2012, **8**, 3056-3061.

44. I. Rayment, H. M. Holden, M. Whittaker, C. B. Yohn, M. Lorenz, K. C. Holmes and R. A. Milligan, *Science*, 1993, **261**, 58-65.

45. Y. Zhang, N. Zhou, S. Akella, Y. Kuang, D. Kim, A. Schwartz, M. Bezpalko, B. M. Foxman, S. Fraden, I. R. Epstein and B. Xu, *Angew. Chem. Int. Ed.*, 2013, **52**, 11494-11498.

46. Y. Zhang, R. Zhou, J. F. Shi, N. Zhou, I. R. Epstein and B. Xu, *Journal of Physical Chemistry B*, 2013, **117**, 6566-6573.

47. Y. Zhang, N. Li, J. Delgado, Y. Gao, Y. Kuang, S. Fraden, I. R. Epstein and B. Xu, *Langmuir*, 2012, **28**, 3063-3066.

48. P. Dayal, O. Kuksenok and A. C. Balazs, *Langmuir*, 2009, **25**, 4298-4301.

49. X. Lu, L. Ren, Q. Gao, Y. Zhao, S. Wang, J. Yang and I. R. Epstein, *Chem. Commun.*, 2013, **49**, 7690-7692.

50. M. F. Crowley and R. J. Field, *Journal of Physical Chemistry*, 1986, **90**, 1907-1915.

51. J. P. Laplante and T. Erneux, *Physica A*, 1992, **188**, 89-98.

52. I. Stuchl and M. Marek, *J. Chem. Phys.*, 1982, **77**, 2956-2963.

53. J. Weiner, R. Holz, F. W. Schneider and K. Bar-Eli, *J. Phys. Chem.*, 1992, **96**, 8915-8919.

54. V. Horvath, P. L. Gentili, V. K. Vanag and I. R. Epstein, *Angew. Chem. Int. Ed.*, 2012, **51**, 6878-6881.

55. R. M. Harris-Warrick, E. Marder, A. I. Selverston and M. Moulin, eds., *Dynamic Biological Networks: The Stomatogastric Nervous System*, MIT Press, Cambridge, MA, 1992.